中國機械工程學會第十屆學術研討會

固力組論文集

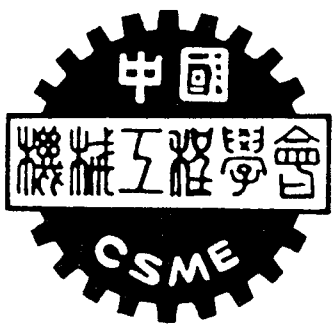

PROCEEDINGS OF THE TENTH NATIONAL
CONFERENCE OF THE CHINESE SOCIETY OF
MECHANICAL ENGINEERS

HSINCHU, TAIWAN
REPUBLIC OF CHINA
DECEMBER, 1993

新竹市　國立交通大學
中華民國八十二年十二月

轉子動力學

振動

Active Control of Far-Field Sound Radiated by a Beam: Physical System Analysis

Bor-Tsuen Wang
Department of Mechanical Engineering
National Pingtung Polytechnic Institute
Pingtung, Taiwan 91207

ABSTRACT

This paper analytically demonstrates the use of piezoelectric actuators and PVDF sensors to actively control the far-field sound radiation through a simply-supported beam with the infinite rigid baffled. The beam is assumed to be subjected to a harmonic point force. The piezoelectric patches which are attached to the beam serve as actuators to control the sound radiated through the beam into the far-field, while the PVDF films serve as structural error sensors. A minimization process is used to calculate the optimal input voltages into the piezoelectric actuators so as to minimize the cost function which is the least mean square (LMS) value of the error sensor signals. Radiation directivity pattern and wavenumber analysis are performed to evaluate the control effectiveness. Results show that the use of the compact distributed types of actuators and sensors can efficiently attenuate the far-field sound radiation. The reduction of sound pressure level for on-resonance cases is over 20-50 dB; however, little attenuation can be achieved or even spillover may occur for off-resonance cases due to the improper location of actuators and sensors. This work demonstrates the use of structural actuators and near-field sensors for far-field sound radiation control and leads to the inherent applications of intelligent material structure system.

Key words: active structural acoustic control, piezoelectric, PVDF

INTRODUCTION

Active structural acoustic control (ASAC) have been drawn a great deal of interest over the past few years. Leug [1] first proposed to cancel the primary sound wave with the use of secondary sound wave 180° out-of-phase with respect to the primary source. The sound source (speaker) which is not a "real" actuator is to apply in the acoustic field to cancel the sound wave. Many researchers have shown the feasibility of sound sources in ASAC [2-5]. An effective way to control the structural sound radiation is to apply control force directly to the radiated structures. Shakers can efficiently control the sound radiation [6-8], although shakers have substantial disadvantages due to their large volume, large weight and requiring support. Recently, the compact distributed types of actuators, such as piezoelectric patches, have been shown feasible for structural vibration and acoustic control [9-12].

Microphones are generaliy used as error sensors in ASAC; however, that microphones must be located in the radiated far-field makes them impractical for applications. Structural sensors, such as accelerometers, have been proposed for ASAC [13]. Although accelerometers overcome the disadvantages of far-field sensors, accelerometers are still impactical for implementation due to the high cost and the difficulty to <xhere to the structure. PVDF sensors which is a film type of sensor attached to the structure has been applied to structural vibration and acoustic control [14,15]. The PVDF sensors are more practical than microphones or accelerometers for applications because of their compactness and low cost.

This paper presents the use of compact distributed piezoelectric actuators and PVDF film sensors for active control of far-field sound radiation through a beam. The simply-supported beam with infinite baffle subjected to a harmonically excited point force is considered as the plant. Both piezoelectric actuators and PVDF sensors are attached to the radiated structure. A linear quadratic optimization process is applied to obtain the optimal control voltages input to the piezoelectric actuators so as to minimize the cost function. The cost function is constructed as the sum of the least mean square value of error sensor signals. The structural response and sound radiation directivity pattern were studied to show the control effectiveness as well as the wavenumber analysis. Results show that sufficient control can be achieved for on-resonance cases. Little reduction of sound pressure level or even spillover may occur for off-resonance cases due to the inappropriate

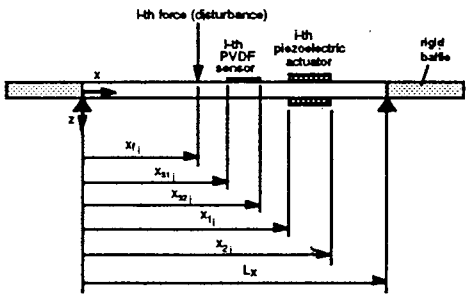

Figure 1. The arrangement and coordinates of simply-supported beam

location of sensors and actuators. The optimization design of actuators and sensors may be required for further study. Nevertheless, this work shows the effectiveness of far-field sound radiation with the use of near-field structural actuators and sensors. This work also leads to an inherent applications of intelligent material structures to the ASAC.

THEORETICAL ANALYSIS

Lateral Vibration of Uniform Beam

Consider a uniform simply-supported beam with length of L, as shown <x Figure 1, the equation of motion can be obtained as follow:

$$E_b I\frac{\partial^4 w}{\partial x^4}+\rho_b b t_b\frac{\partial sup Hxw}{\partial t^2}-p(x,t) \tag{1}$$

where E_b is the Young's modulus of the beam; I the moment of inertia; ρ_b the beam density; t_b the beam thickness; b the beam width; $p(x,t)$ the force function. Note that the damping effect is assumed small and can be neglected for simply application. The boundary condition for a simply-supported beam are

$$M(0,t)-M(L,t)-E_b I\frac{\partial^2 w}{\partial x^2}-0 \tag{2}$$

$$w(0,t)-w(L,t)-0 \tag{3}$$

For free vibration analysis, i.e., $p(x,t)-0$, the natural frequencies can be found to be

$$\omega_n-(n\pi)^2\sqrt{\frac{E_b I}{\rho_b b t_b L^4}} \tag{4}$$

The general form of beam lateral displacement, while the beam is subjected to harmonic force inputs, can be written as the follow:

$$w(x,t)-e^{i\omega t}\sum_{n-1}^{\infty} W_n \sin\alpha_n x \tag{5}$$

where

$$\alpha_n-\frac{n\pi}{L} \tag{6}$$

$$W_n-\frac{P_n}{\rho_b b t_b(\omega_n^2-\omega^2)} \tag{7}$$

Here ω is the excitation frequency; α_n is the modal number; W_n is the modal amplitude; and P_n is the modal force depending on the forms of external forces.

Point Force Excitation:

For a harmonic point force with the amplitude of F located at x_f acting on the beam, the force function, p(x,t), can be written as follow:

$$p(x,t)-F\delta(x-x_f)e^{i\omega t} \tag{8}$$

The Delta function, $\delta(x)$, is employed to represent the location of the point force. The modal force, P_n^f, due to the point force excitation is given as follow:

$$P_n^f-\frac{2F}{L}\sin\alpha_n x_f \tag{9}$$

where the superscript f signify the point force.

Piezoelectric excitation:

For an actuator consisting of two identical piezoceramic patches bonded symmetrically on the two opposite beam surfaces and activated 180° out-of-phase, the equivalent external forces can be derived as follow [16]):

$$p(x,t)-M_{eq}[\delta'(x-x_1)-\delta'(x-x_2)]e^{i\omega t} \tag{10}$$

where

$$M_{eq}-C_0\Lambda-\frac{t_b^2 E_b}{6}Kb_a\Lambda \tag{11}$$

$$K-\frac{6}{6+\Psi} \tag{12}$$

$$\Psi-\frac{E_b t_b}{E_a t_a} \tag{13}$$

$$\Lambda-\frac{d_{31}}{t_a}V \tag{14}$$

$C_0\Lambda$ is the equivalent moment induced by the piezoelectric patches attached to the top and bottom of the beam and excited 180° out-of-phase. Λ is the strain induced by an unconstrained piezoelectric layer of thickness, t_a, when a voltage V is applied along its polarization direction, while d_{31} is the piezoelectric dielectric strain constant. Ψ is the effective stiffness ratio. t_a and E_a are the thickness and Young's modulus of the piezoelectric patch respectively. The resultant force is, in fact, the concentrated moments acting on the both edges of piezoelectric patches represented by the first derivative of Delta function. The corresponding expression of modal force for piezoelectric excitation, P_n^c, can be deriv<x [16] as follow:

$$P_n^c = \frac{2M_{eq}}{L}\alpha_n(\cos\alpha_n x_1 - \cos\alpha_n x_2) \tag{15}$$

where x_1 and x_2 are the coordinates of the piezoelectric actuator, and the superscript c signify the control force.

PVDF sensors' equations

For a PVDF film arranged as shown in Figure 1, the shape function can be expressed as follow:

$$\Gamma(x) = u(x-x_{s1}) - u(x-x_{s2}) \tag{16}$$

where $u(x)$ is the step function; x_{s1} and x_{s2} are the coordinates of the PVDF film. The sensor's equation can then be derived as follows [17]:

$$q(t) = -\frac{t_b+t_s}{2} b_s e_{31} \int_0^L \Gamma(x)\frac{\partial^2 y}{\partial x^2}dx \tag{17}$$

where b_s is the sensor width; t_s the sensor thickness; e_{31} the piezoelectric field intensity constant. By substituting $w(x,t)$ and integrating over the beam length,

$$q(t) = e^{i\omega t}\left(\frac{t_b+t_s}{2} e_{31} b\right)\sum_{n=1}^{\infty} \alpha_n W_n(\cos\alpha_n x_{s2} - \cos\alpha_n x_{s1}) \tag{18}$$

The generated voltages can then be expressed as:

$$V(t) = -\frac{q(t)}{\varepsilon A} t_s \tag{19}$$

where ε is the permittivity of PVDF films; A is the sensor area. It is noted that the generated voltage is proportional to the slope difference between the two edges of a PVDF film.

Sound Radiated in the Far-Field

The far-field sound pressure radiated from a vibrating surface at a point in the acoustic field, as shown in Figure 2, is given by the Rayleigh integral [18]:

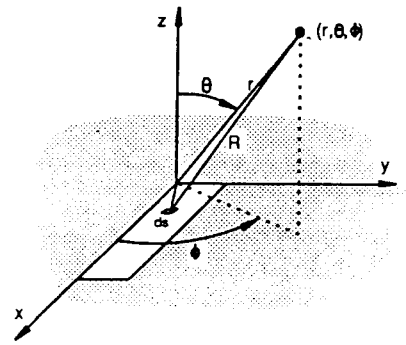

Figure 2. Sound radiated coordinates system

$$p(\vec{r},t) = -\frac{i\omega\rho}{2\pi}\int_s \dot{w}(\vec{r}_s)\frac{e^{-i\kappa R}}{R}ds \tag{20}$$

where $\vec{r}$ is the position vector of the observation point; $\vec{r}_s$ is the position vector of the elemental surface ds; $\dot{w}(\vec{r}_s)$ is the normal velocity of ds; R is $|\vec{r}-\vec{r}_s|$; ρ is the fluid density; and $\kappa = \omega/c$ is the acoustic wavenumber. Here, the acoustic medium is air, and thus there is no feedback of the fluid motion into the structure. By substituting the beam velocity derived from Equation (5) into the Rayleigh integral, the sound pressure radiated to the far-field can be obtained [19]:

$$p(r,\theta,\phi,t) = e^{i\omega t}\sum_{n=1}^{\infty} W_n q_n \tag{21}$$

where

$$q_n = -i\omega\frac{\rho c b}{\pi}\frac{\kappa}{\alpha_n}\frac{e^{-i\kappa r}}{2r}\left[\frac{1-(-1)^n e^{-i\alpha}}{1+(\alpha/n\pi)^2}\right]\left[\frac{1-e^{-i\beta}}{\beta}\right] \tag{22}$$

$$\alpha = \kappa L\sin\theta\cos\phi \tag{23}$$

$$\beta = \kappa b\sin\theta\sin\phi \tag{24}$$

Under the assumption of superposition, the total radiated sound pressure can be the sum of sound pressures due to the disturbance and control inputs

$$p_t = p_f + p_c = e^{i\omega t}\sum_{n=1}^{\infty}(W_n^f + W_n^c)q_n \tag{25}$$

The total radiated sound power defined as the integral of the square of the radiated sound pressure over the hemisphere of the radiating field can then be obtained:

$$\Phi_p = \frac{1}{2\rho c}\int_S |p_t|^2 dS = \frac{r^2}{2\rho c}\int_0^{2\pi}\int_0^{\pi/2} |p_t|^2 \sin\theta d\theta d\phi \tag{26}$$

The total radiated sound power can be an index to evaluate the effectiveness of sound radiation control.

Wavenumber Analysis

The beam velocity distribution can be taken Fourier integral transform in κ-plane.

$$\tilde{V}(\kappa_x,\kappa_y)=\int_{-\infty}^{\infty}\int_{-\infty}^{\infty}\dot{w}(x)e^{-i(\kappa_x x+\kappa_y y)}dxdy \tag{27}$$

where

$$\kappa_x=\kappa\sin\theta\cos\phi \tag{28}$$

$$\kappa_y=\kappa\sin\theta\sin\phi \tag{29}$$

the<xfore, the velocity transform can be expressed as:

$$\tilde{V}(\kappa_x,\kappa_y)=i\omega\sum_{n=1}^{\infty}W_n V_n \tag{29}$$

where

$$V_n=i\alpha_n\left[\frac{1-(-1)^n e^{-i\kappa_x L}}{\alpha_n^2-\kappa_x^2}\right]\left[\frac{e^{-i\kappa_y b}-1}{\kappa_y}\right] \tag{30}$$

It is noted that the least mean square (LMS) value of the velocity transform, i.e., $|\tilde{V}|^2$, is proportional to the radiated sound power [18]. Only the wavenumber components satisfying $\kappa_x^2+\kappa_y^2<\kappa^2$ contribute to sound radiation into the far-field and are termed as supersonic waves. Others wavenumber components do not radiate into the far-field and are termed subsonic waves.

LQOCT for PVDF sensors

For N_s PVDF sensors, the cost function can be defined as the sum of the mean square voltages measured from the PVDF films:

$$\Psi_v=\sum_{j=1}^{N_s}|V_j|^2 \tag{31}$$

The linear quadratic optimal control theory (LQOCT) can then be applied to minimize the cost function so as to find the optimal control voltages input to the piezoelectric actuators. The full analysis can be referred to [20] and omitted here for brevity. The vibrating energy of the beam can be expressed as follow:

$$\Phi_w=\int_0^L \bar{w}^2 dx \tag{32}$$

Table 1. Physical properties of the G-1195 piezoceramic patch [21]

$E_a=6.3\times10^{10}(N/m^2)$	$\rho_a=7650\ (Kg/m^3)$
$t_a=1.905(mm)$	$\nu_a=0.28$
$d_{31}=d_{32}=166\times10^{-12}(\frac{m}{volt})$	

Table 2. Physical properties of the PVDF films (LDT-28 μk) [22]

$E_s=2\times10^9(N/m^2)$	$\rho_s=1800\ (Kg/m^3)$
$t_s=28\times10^{-6}(m)$	$\nu_s=0.33$
$e_{31}=54\times10^{-3}(C/m)$	$\epsilon=106\times10^{-12}(F/m)$

which can used as an index to evaluate the effectiveness of vibration control.

NUMERICAL RESULTS AND DISCUSSIONS

A steel beam with length of 0.38m, width of 0.04m, and thickness of 2mm is used in the simulations. The first few natural frequencies are 33.2 Hz, 128.8 Hz, 289.9 Hz, 515.4 Hz, 805.3 Hz and 1159.6 Hz. It is noted that no damping was included in the following analysis. The optimal process is suitable for controlling multiple primary sources; however, only one harmonic point force with input parameters, F=0.1N and x_f=0.067m, was considered for the following analysis. The physical properties of the piezoelectric patch (G-1195) [21] and PVDF films (LDT-28 μk) [22] are respectively shown in Tables 1 and 2. The piezoceramic patch is located at x_1=0.285m, x_2=0.3485m, and the PVDF film is located at x_{s1}=0.10m, x_{s2}=0.14m. In order to calculate the beam response and radiated sound pressure, it was necessary to truncate the modal sums in Equation (5). Upon consideration of computing time and accuracy, the first 10 modes were considered, and it was found to provide sufficient convergence of series.

Both the radiation directivity and beam displacement distributions were shown to demonstrate the control effectiveness of sound radiation through the beam. The radiated sound pressure is plotted in dB re 20×10^{-6} Pa over $\theta=-90°$ to $90°$, while the beam displacement distribution is normalized by the largest amplitude in each case and plotted in dB along the beam length.

Figure 3 shows the radiation directivity for the first

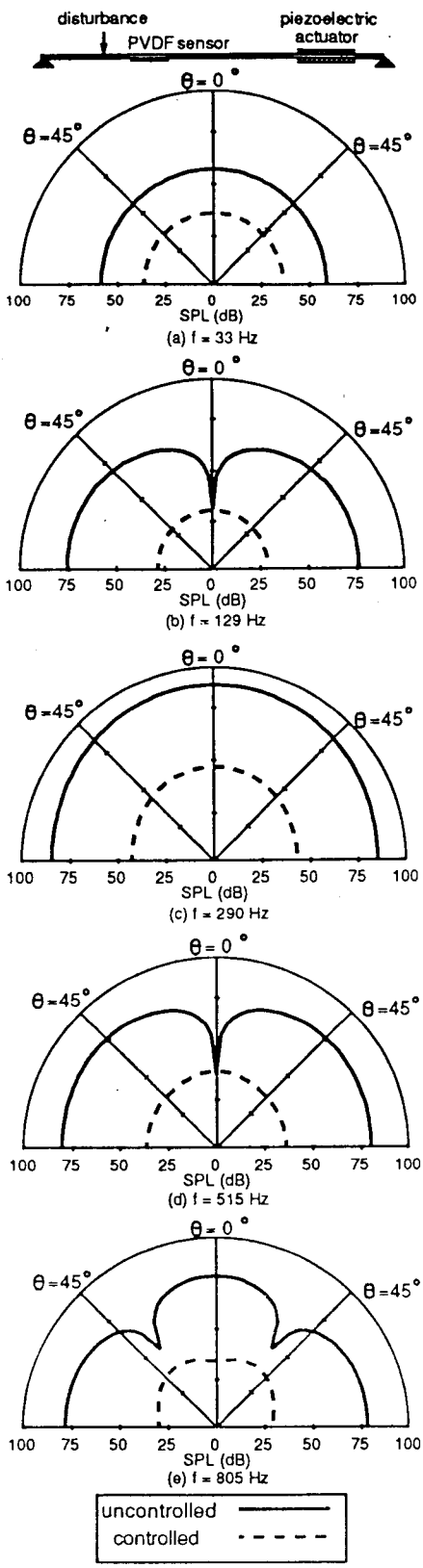

Figure 3. Radiation directivity pattern for (a) first, (b) second, (c) third, (d) fourth, and (e) fifth mode excitation

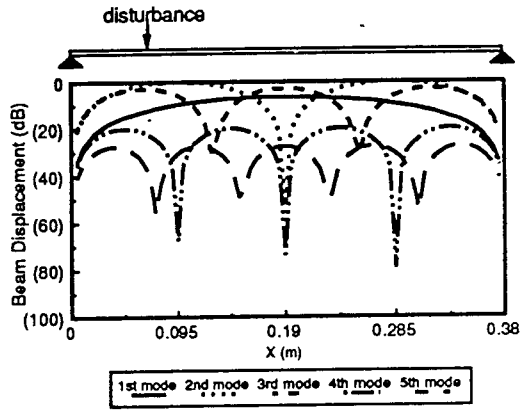

Figure 4. uncontrolled displacement distrbutions for on-resonace excitation

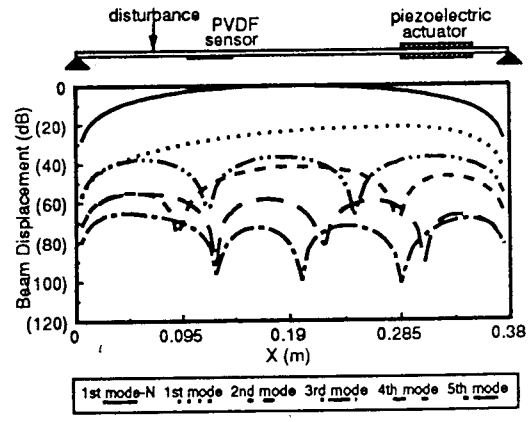

Figure 5. controlled displacement distrbutions for on-resonace excitation

five resonance mode excitation cases. The arrangement of the actuator and sensor is depicted on the top of the figure. The solid line indicates the uncontrolled response. As shown in Figure 3(a), the directivity pattern is uniform for the first mode excitation, while the directivity pattern appears a dip at θ=0° for the second mode excitation as shown in Figure 3(b). For the third mode excitation case, the directivity pattern does not appear a third-mode-like response; however, that the directivity is not uniform evidences the existence of the third mode. Also, the fifth modeHxxcitation gives a third-mode-like response as shown in Figure 3(e). This unmatched mode shape radiation characteristics can be explained in the latter wavenumber analysis. The controlled directivity pattern is denoted by the dashed line. A global reduction of sound pressure level over 20-50 dB can be observed for all of the on-resonance excitation cases. The residual radiation directivity pattern appears a lower mode shape. This indicates that the significant radiated mode is effectively controlled leaving the insignificant modal response.

Table 3. Results for the on-resonance excitation cases

excitation frequency (Hz)	reduction of Φ_w (dB)	reduction of Φ_p (dB)	control voltages (volts)
33	22.1	22.3	-31.9
129	50.5	39.1	8.8
290	40.9	42.2	-4.0
515	44.2	38.4	2.3
805	47.2	43.2	-1.3

Table 4. Results for the off-resonance excitation cases

excitation frequency (Hz)	reduction of Φ_w (dB)	reduction of Φ_p (dB)	control voltages (volts)
80	0.6	-1.0	6.6
210	-3.3	-0.9	5.6
400	-8.0	-6.6	7.5
660	-0.5	-0.4	-3.4

The beam displacement distributions due to the disturbance alone for the first five resonance mode excitation cases are shown in Figure 4. The second mode excitation gives the highest response because of the location of the point force disturbance. As seen in Figure 4, the third mode structural response is smaller than the second mode structural response; however, the radiated sound pressure level for the third mode excitation case is higher than that for the second mode excitation case as shown in Figures 3(b) and 3(c). It is because that the odd mode is the more efficient radiator than the even mode. This can also be further explained by the wavenumber analysis. The controlled beam displacement distributions for on-resonance excitation corresponding to the cases in Figure 3 are shown in Figure 5 for comparison. The residual beam response is found to be globally reduced for each case.

To further examine the radiation characteristics of the beam, a wavenumber analysis as shown previously is performed. The LMS value of velocity transform plotted over the structural wavenumber (κ_x) is shown in Figure 6 for the on-resonance excitation cases when κ_y=0, and the acoustic wavenumber ($\kappa=\omega/c$) is also indicated. The wavenumber components satisfying $-\kappa<\kappa_x<\kappa$ which contributes to the far-field sound radiation is characterized as the supersonic region [18]. Other wavenumber components, i.e., $|\kappa_x|>\kappa$, which do not radiate is termed as the subsonic region. For odd mode excitations, that the LMS value of the velocity transform appears a peak at κ_x=0 makes the structure an efficient radiator. Conversely, for the even mode excitation a dip at κ_x=0 makes the structure an inefficient radiator. One can also observe that the shape of the radiation directivity shown in Figure 3 is related to the velocity transform in Figure 6. The radiation mode shape appears in the directivity pattern exactly the same as the number of modes involved in the supersonic region. As control applied, the LMS value of velocity transform is globally reduced over the wide range of the structural wavenumber. In particular, the reduction of the LMS value of velocity transform in the supersonic region implies the reduction of radiated power as mentioned previously.

Table 3 summarizes the results of on-resonance excitation cases. Φ_p which is the total radiated sound power of the beam can be an index for evaluating the effectiveness of sound radiation control, while Φ_w which is the vibrating energy can be an index for evaluating the effectiveness of vibration control [20]. The large amount of reduction of Φ_w does not imply the equivalent amount of reduction of Φ_p. The amount of radiated sound power depends on the structural mode shape as well as the edge effect [23]. It is worth to mention that for the second mode excitation case with control, the reduction of Φ_w is up to 50.5 dB; however, the reduction of Φ_p is only about 39.1 dB. It is because that the residual beam response, as shown in Figure 5, is a third-mode-like mode shape which is an efficient radiator as discussed previously.

Figure 7 shows the radiation directivity for off-resonance excitation cases. One can observe that little reduction of sound pressure level is achieved or even spillover occur. This can be due to the inappropriate location of the actuator and sensor. The uncontrolled and controlled beam displacement distributions for off-resonance excitation cases are shown in Figures 8 and 9 respectively. One can observed that the beam response is not reduced as control applied, and the shape of radiation directvity is corresponding to the structural response of the beam. The wavenumber analysis for the off-resonance excitation cases is shown in Figure 10. The wavenumber components in the supersonic region is not reduced. In particular, as shown in Figure 10(b) for f=210Hz, some wavenumber components are attenuated; however, there are more spillover in the supersonic region. As shown in Table 4, the negative value of reduction of reduction of Φ_p indicates the insufficient sound radiation control. To cure the control defect of off-

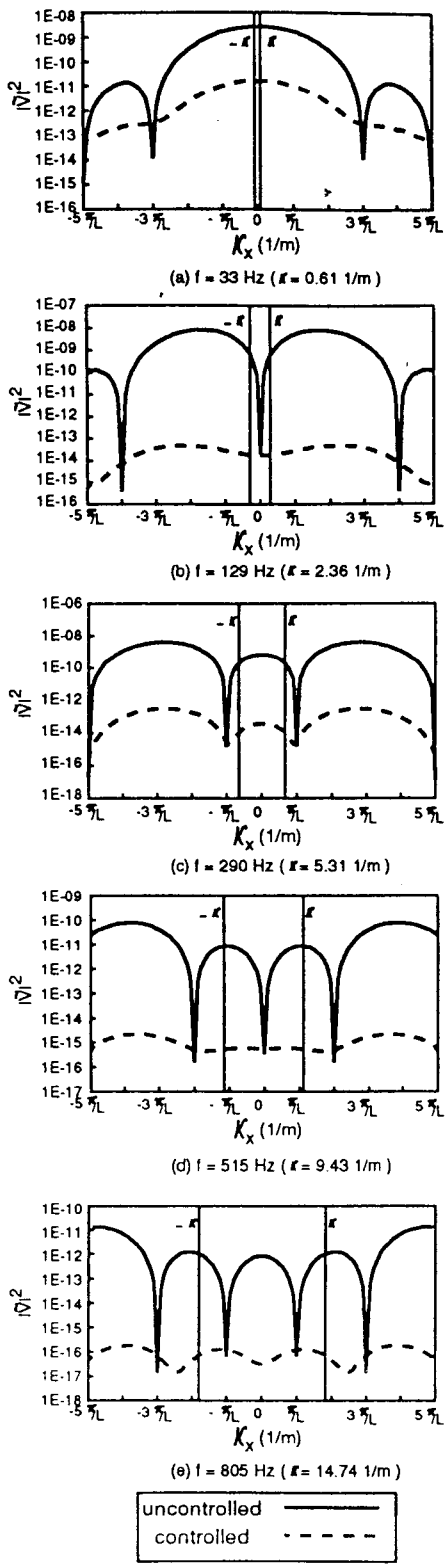

Figure 6. LMS value of velocity transform for (a) first, (b) second, (c) third, (d) fourth, and (e) fifth mode excitation

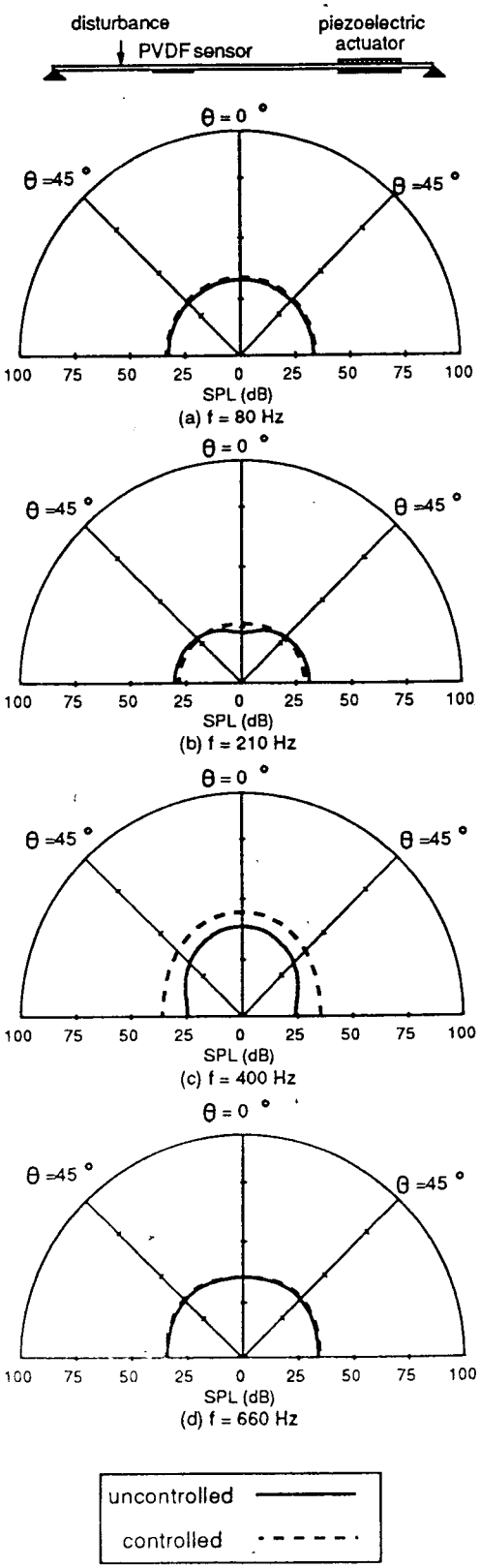

Figure 7. Radiation directivity pattern for off-resonance excitation

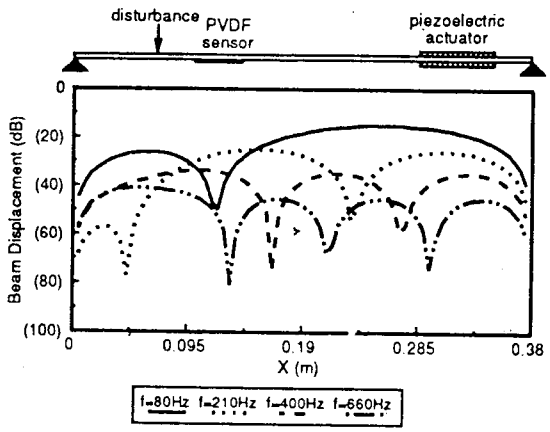

Figure 8. uncontrolled displacement distrbutions for off-resonance excitation

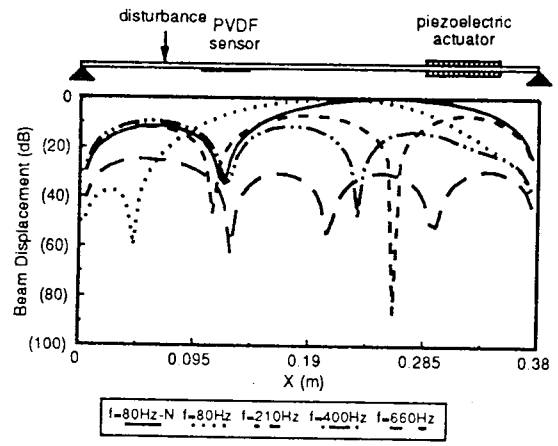

Figure 9. controlled displacement distrbutions for off-resonance excitation

resonance excitation case, the appropriate number and location of actuators and sensors must be selected; however, the optimal placement of actuators and sensors is out of the content of this paper. The optimization problem regarding to the placement of actuators and sensors is currently investigated in NPPI. The alternative solution may also construct an efficient cost function, such as the LMS value of the velocity transform, in order to achieve the sufficient control for off-resonance excitation cases.

CONCLUSIONS

This paper demonstrates the application of piezoelectric actuators and PVDF sensors to the active structural acoustic control in conjunction with the use of the LMS feedforward control. Results show that PVDF film is a suitable near-field structural sensor for the ASAC in the replacement of the traditional far-field microphone error sensor. In particular, the effective control can be achieved for on-resonance excitation cases, and the radiated sound power can be attenuated over 20-40 dB. The radiation

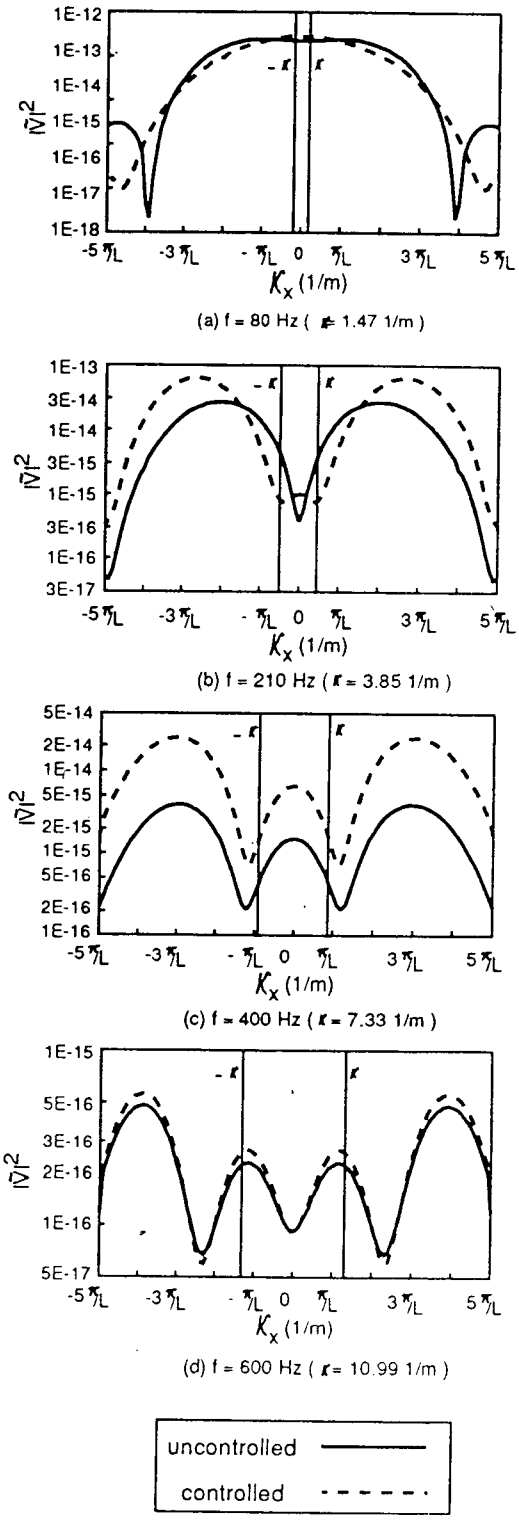

Figure 10. LMS value of velocity transform for off-resonance excitation

directivity and the beam displacement distribution were presented to show the characteristics of active sound radiation control. An extensive wavenumber analysis was also performed and shown to be an effective mean to study the sound radiation mechanism. For off-resonance excitation cases, little control can be achieved or even spillover occurs due to the improper location of the actuator and sensor; therefore, a future study on the optimal placement of piezoelectric actuators and PVDF sensors may be needed in order to achieve sufficient control. The alternative solution may be to reconstruct the cost function based on the wavenumber domain sensors which can effectively reduce the supersonic wave components. In summary, this work provides a theoretical analysis for distributed types of actuators and sensors in ASAC and leads to an efficient design of intelligent material structure system.

ACKNOWLEDGEMENTS

The author gratefully acknowledges the support of the work by National Science Council, Republic of China, under grant NSC82-0410-E-020-001.

REFERENCES

1. Lueg, 1936, "Process of Silencing Sound Oscillator," U.S. Patent No. 2,043,416.
2. Lester, H. C., and C. R. Fuller, 1990, "Active Control of Propeller Induced Noise Fields Inside a Flexible Cylinder," AIAA Journal, **28(8)**, pp. 1374-1380.
3. Deffayet, C., and P. A. Nelson, 1988, "Active Control of Low Frequency Harmonic Sound Radiated by a Finite Panel," Journal of the Acoustical Society of America, **84(6)**, pp. 2192-2199.
4. Nelson, P. A., A. R. D. Curtis, S. J. Elliott, and A. J. Bullmore, 1987, "The Active Minimization of Harmonic Enclosed Sound Fields, Part I: Theory," Journal of Sound and Vibration, **117(1)**, pp. 1-13.
5. Song, L. , G. H. Koopmann, and J. B. Fahniline, 1991, "Active Control of the Acoustic Radiation of a Vibrating Structure Using a Superposition Formulation," Journal of the Acoustical Society of America, **89(6)**, pp. 2786-2792.
6. Jones, J. D., and C. R. Fuller, 1989, "Active Control of Sound Fields in Elastic Cylinders by Multiple Forces," AIAA Journal, **27(7)**, pp. 845-852.
7. Meirovitch, L., and S. Thangjitham, 1990, "Control of Sound Radiation Pressure," Journal of Vibration and Acoustics, **112(2)**, pp. 237-244.
8. Pan, J., C. H. Hansen, and P. A. Bies, 1990, "Active Control of Noise Transmission through a Panel into a Cavity: I. Analytical Study," Journal of the Acoustical Society of America, **87(5)**, pp. 2098-2108.
9. Wang, B.-T., C. R. Fuller, and E. K. Dimitriadis, 1991, "Evaluation of Active Control of Noise Transmission Through Rectangular Plates Using Multiple Piezoelectric or Point Force Actuators," Journal of Acoustical Society of America, **90(5)**, pp. 2820-2830.
10. Burdisso, R. A., and C. R. Fuller, 1992, "Dynamic Behavior of Structural Acoustic Systems in Feedforward Control of Sound Radiation," Journal of Acoustical Society of America, **92(1)**, pp. 277-286.
11. Dimitriadis, E. K., C. R. Fuller, and C. A. Rogers, 1991, "Piezoelectric Actuators for Distributed Vibration Excitation of Thin Plates," Journal of Vibration and Acoustics, **113**, pp. 100-107.
12. Wang, B.-T., E. K. Dimitriadis, and C. R. Fuller, 1991, "Active Control of Structurally Radiated Noise Using Multiple Piezoelectric Actuators," AIAA Journal, Vol. 29, No. 11, pp. 1802-1809.
13. Fuller, C.R., J. D. Jones, 1987, "Influence of Sensor and Actuator Location on the performance of Active Control System," 87-WA/NCA-9, ASME Annual Meeting, Boston, Massachusetts.
14. Clark, R. L., C. R. Fuller, 1991, "Control of Sound Radiation with Adaptive Structures," Journal of Intelligent Material System and Structures, **2(3)**, pp. 431-452.
15. Clark, R. L., C. R. Fuller, 1992, "A Model Reference Approach for Implementing Active Structural Acoustic Control," Journal of Acoustical Society of America, **92(3)**, pp. 1534-1544.
16. Wang, B. T., and C. A. Rogers, 1991, "Modeling of Finite-Length Spatially Distributed Induced Strain Actuators for Laminate Beams and Plates," Journal of Intelligent Material System and Structures, **2(1)**, pp. 38-58.
17. Lee, C. K., and F. C. Moon, 1990, "Modal Sensors/Actuators," Journal of Applied Mechanics, **57(2)**, pp. 434-441.
18. Fahy, F., 1985, Sound and Structural Vibration, Academic, Orlando, Florida.
19. Wallace, C. E., 1972, "Radiation Resistance of a Baffled Beam," Journal of Acoustical Society of America, **51(3)**, pp. 936-945.
20. Wang, B.-T., 1992, "A Dynamic Simulation of Hybrid Active and Passive Control of Structural Vibration," NSC Report, NSC81-0401-E-020-501.
21. Piezo Systems, Inc., 1990, Product Catalog.

22. Pennwalt Corporation, 1990, Piezo Film Sensor Application Notes.

23. Peng, H. and P. B. Lees, 1990, "Edge Effect in Radiation Efficiency of a Baffled Beam Below the Critical Frequency," Journal of Acoustical Society of America, **88(4)**, pp. 2001-2006.

樑之遠場聲音輻射的主動控制：系統分析

王柏村
國立屏東技術學院
機械工程技術系

本篇報告說明使用壓電驅動器及壓電薄膜感應器去主動控制無限長剛體屏障的簡支樑之遠場聲音輻射，樑假設受到簡諧激振之點力干擾源，壓電材料黏貼在樑上作驅動器以控制樑之遠場聲音輻射，壓電薄膜則作為結構之感應器，應用一求最小值方法，來計算最佳之壓電驅動器輸入電壓，使能將成本函數最小化，此成本函數為感應器信號之最小平方值。分別作輻射指向圖和波數分析以評估控制效果，結果顯示，使用此精簡均佈式驅動器及感應器能有效減小遠場之聲音輻射，在共振激振時，可減小聲壓位階20～50dB，但是在非共振激振時，聲壓減小很少，甚至會有盈溢現象，乃由於不適當的驅動器及感應器位置，本文証明使用結構型驅動器及近場的感應器作遠場聲音輻射控制之有效性，更為智慧型材料結構系統之潛在應用。

關鍵字：主動結構噪音控制，
壓電驅動器，壓電薄膜